Predictive Models with Patient Specific Material Properties for the Biomechanical Behavior of Ascending Thoracic Aneurysms

Olfa Trabelsi[1], Ambroise Duprey, Jean-Pierre Favre, Stéphane Avril

Predictive models with patient specific material properties for the biomechanical behavior of ascending thoracic aneurysms

Olfa TRABELSI[1,*], Ambroise DUPREY[1,2], Jean-Pierre FAVRE[2], Stéphane AVRIL[1]

[1] Center for Biomedical and Healthcare Engineering, Ecole Nationale Supérieure des Mines de Saint-Etienne, CIS-EMSE, CNRS:UMR5307, LGF, Saint Etienne, France. (olfa.trabelsi@emse.fr)

[2] Hôpital Nord, Cardiovascular Surgery Service, CHU de Saint Etienne, F-42055 Saint-Etienne, France.

ABSTRACT

The aim of this study is to identify the patient-specific material properties of ascending thoracic aortic aneurysms (ATAA) using preoperative dynamic gated Computed Tomography (CT) scans. The identification is based on the simultaneous minimization of two cost functions, which define the difference between model predictions and gated CT measurements of the aneurysm volume at respectively systole and cardiac mid-cycle.

The method is applied on 5 patients who underwent surgical repair of their ATAA at the University Hospital Center of St. Etienne. For these patients, the aneurysms were collected and tested mechanically using an in vitro bench. For the sake of validation, the mechanical properties found using the in vivo approach and the in vitro bench were compared. We eventually performed finite-element stress analyses based on each set of material properties. Rupture risk indexes were estimated and compared,

showing promising results of the patient-specific identification method based on gated CT.

Keywords: ATAA, mechanical properties, inverse method, rupture risk.

I. INTRODUCTION

Ascending thoracic aortic aneurysm (ATAA) is a local dilatation in the aortic wall that may affect people independently of age and gender [23]. Most ATAAs are asymptomatic and are only detected as incidental findings during the investigation of other conditions. Spontaneous rupture of an ATAA is almost always fatal; therefore treatment is focused on timely surgery to prevent rupture [5,6,7,8,14,23,24,50]. The maximum diameter of an aneurysm has long been the preferred clinical method for assessing rupture risk. Surgical intervention is indicated for aneurysms with diameters larger than 5.5 cm or for fast growing aneurysms (> 1 cm per year) [5,6,7,8,14,23,24]. However, studies on abdominal aortic aneurysms (AAA) indicate that biomechanical factors, such as peak wall stress, may estimate the risk of rupture better than the diameter criterion [15, 33, 56]. The use of these biomechanical factors in the prediction of AAA rupture risks has been shown to be very promising [12,13,15,33]. However, rupture risk estimation requires performing a patient-specific finite-element (FE) stress analysis which usually needs the following inputs: patient specific geometries, patient specific thicknesses, patient specific material properties, patient specific blood actions and patient specific wall strengths. Obtaining these inputs non-invasively for each patient represent important challenges.

CT scans (systematically available before any surgical repair of an ATAA) and MRI scans (seldom available) are commonly used for the reconstruction of patient specific geometries [20,40,59]. Regarding patient specific blood actions, 4D MRI can even

provide information on the regional hemodynamic action in the aorta [19,29,41]. Obtaining the local thickness is still challenging, despite the importance of this parameter for AAAs and ATAAs [37,44, 49].

The current study is focused on identifying, non-invasively and in vivo, the patient specific material properties of ATAAs, which represent essential biomechanical determinants for ATAA strength [2,11,26] and for ATAA growth [31,32,49,60].

Several inverse approaches have already been developed to estimate mechanical properties of soft tissues in the human body [1]. Most of them try to minimize a cost function defined as the deviation between a target metric which is obtained from measured images, and a candidate metric which is obtained with a FE model and which is iteratively updated by tuning the mechanical constitutive properties of the proposed model. Updating may be achieved through different optimization algorithms, ranging from simplex methods [35] to evolutionary algorithms [30]. It is always important to verify the uniqueness of the obtained solution [3].

Different candidates for the metric may be local deformations [53], strains [18], cross section areas or volumes [17,18,27,30]. Few have used the volume occupied by a given constituent, because most soft tissues are incompressible and do not show bulk volume variations above the resolution of imaging techniques. However, the variations of the volume occupied by the lumen of the aorta may be a good metric to identify the mechanical properties of the wall as significant luminal volume variations occur throughout cardiac cycles due to pressure variations and induced stretch variations in the vessel wall [17,18].

Accordingly, in this study, we propose an inverse method to identify the patient-specific material properties of the ATAA using volume variations of the dynamic CT

scans. The inverse method is based on the simultaneous minimization of two cost functions which define the difference between model predictions and CT measurements of the aneurysm volume change at respectively systolic pressure and cardiac mid-cycle, with respect to the diastolic volume (reference volume).

In this proof-of-concept study, model predictions were obtained with simplified FE models of ATAAs: only the ascending part of the aorta (between the aortic root and the aortic arch) was modelled, a uniform thickness and uniform material properties were assumed for each patient, the blood action was limited to a uniform luminal pressure neglecting the perivascular pressure, and the length of the modelled aortic segment was maintained constant during pressure changes.

The method was applied on 5 patients who underwent surgical repair of their ATAA at the University Hospital Center of St. Etienne (CHU-SE). For these patients, the aneurysms were collected and tested mechanically using an *in vitro* bench. For the sake of validation, the mechanical properties found using the *in vivo* inverse approach and the *in vitro* experimental tests were compared. FE stress analyses on the patient specific geometries and with each set of material properties were eventually performed. The peak wall stress and the overpressure index (ratio between the actual systolic pressure and the burst pressure of the artery) obtained with both sets of material properties were always found similar.

II. MATERIALS AND METHODS

1. Constitutive model of ATAA based on experimental study.

ATAA specimens and pre-operative ECG gated dynamic CT scans were obtained from five patients undergoing elective surgery for ATAA repair at CHU-SE, between

December 2012 and March 2013. Their demographic information and medical history is reported in Table 1.

Table 1. Patient demographic information

Patient ID	Sex/Age	Pre-surgical CT diameter (mm)	Pathologies	CT scan date	Blood pressure	
					Date	Max/min (mmHg)
1	M/55	55	AI, bicuspid aortic valve	20/02/2013	29/01/2013	122/78
					18/03/2013	123/87
2	F/76	65	AI	-	-	-
3	M/79	52	AI, coronary artery disease, myocardial infarction	-	-	-
4	M/40	55	AI, bicuspid aortic valve	30/11/2012	03/12/2012	112/69
					04/12/2012	135/88
5	M/72	51	AI, coronary artery disease, hypertension	19/12/2012	03/12/2012	174/87
					04/12/2012	126/64
						139/66

Aortic insufficiency (AI)

The material properties were determined by performing bulge inflation tests on the collected aneurysm samples. The Institutional Review Board of CHU-SE approved the use of human tissue and all data collection in this study. Specimens were kept at 4°C in 0.9% physiological saline solution and all mechanical tests were completed within 24h after tissue harvest, except for patient 4 whose specimen was tested after 48h of the surgical repair. For each patient, ten measures of the wall thickness have been taken on each ATAA sample following the method described by [25, 37], and the average value for each patient has been reported in Table 2. The tissue was then tested according to our previously published protocol [47]. Briefly, a 45 mm square sample was cut from the greater curvature of each ATAA specimen and clamped in a bulge inflation device. During the bulge inflation test, water at a constant rate was injected by pushing a piston pump at 15 mm/min until the tissue ruptured (Figure 1). Simultaneously, the pressure was measured using a digital manometer (WIKA, DG-10) and images were recorded using a commercial stereo-digital image correlation (DIC) system (GOM, 5M LT). The collected images were analysed using ARAMIS

(GOM, v. 6. 2.0) to measure the three dimensional displacement of the tissue surface.

From the displacement fields, Green-Lagrange strains were derived and Cauchy stresses were reconstructed using the inverse membrane approach [47]. In another study [54], we showed that the Demiray constitutive model [10] offers a reasonable description of the average elastic response of the ATAA across the tested area. The strain energy density function for the Demiray model may be written:

$$W = \kappa(J-1)^2 + D_1\left(e^{D_2(\overline{I_1}-3)} - 1\right), \qquad (1)$$

where the deformation gradient, $\mathbf{F} = J^{1/3}\,\mathbf{I}\,\overline{\mathbf{F}}$, has been decomposed into its dilatational and isochoric parts and $\overline{\boldsymbol{C}} = \overline{\mathbf{F}}^{T}\overline{\mathbf{F}}$ is the modified right Cauchy-Green tensor. The strain energy depends on the local volume ratio, $J = \det(\boldsymbol{F})$, and $\overline{I_1} = \mathrm{tr}\,\overline{\mathbf{C}}$. The parameter D_1 has units of stress whereas D_2 is dimensionless, and κ is the compressibility modulus. The second Piola-Kirchhoff stress is then given by:

$$S = 2\,\frac{\partial W}{\partial C} = 2\kappa J(J-1)\mathbf{C}^{-1} + J^{-2/3}\left(\mathbb{I} - \frac{1}{3}\mathbf{C}^{-1}\otimes\mathbf{C}\right) : \left(2D_1D_2\, e^{D_2(\overline{I_1}-3)}\right)\mathbf{I} \qquad (2)$$

where $\mathbb{I}$ is the fourth order identity tensor.

The value of the model parameter κ was set to 1 GPa to approximate the nearly incompressible response of the ATAA [4, 43]. The average values of D_1 and D_2 identified for each patient in our previous works are reported in Table 2.

Table 2. Patient specific material properties identified using the bulge-inflation test and aneurysm CT volumes variation (ΔV) at systole and cardiac mid-cycle with respect to the diastole (reference).

Patient ID	D_1 (kPa)	D_2	ε	Ex-vivo thickness (mm)	Rupture Stress (MPa)	CT systolic ΔV(%)*	CT mid-cycle ΔV(%)*

1	$8.684^{+0.211}_{-0.205}$	$2.031^{\pm 0.027}$	0.041	2.38	1.05 (n=2)	12.98	5.25
2	$1.766^{+0.081}_{-0.078}$	$6.932^{+0.194}_{-0.19}$	0.034	2.44	1.31 (n=4)	1.80	1.03
3	$4.722^{+0.196}_{-0.191}$	$9.131^{+0.359}_{-0.356}$	0.088	1.76	0.95 (n=1)	2.46	0.99
4	$9.397^{+0.305}_{-0.299}$	$1.972^{\pm 0.031}$	0.063	1.59	2.33 (n=2)	14.64	5.57
5	$10.33^{+0.31}_{-0.29}$	$5.265^{+0.138}_{-0.135}$	0.030	1.90	0.76 (n=2)	18.76	11.27

*The volume variation is calculated with respect to the diastole (reference).

2. Computational Study

For each patient, ECG gated dynamic CT scans were processed to reconstruct the aneurysm geometry during the cardiac cycle, including diastole and systole. For each patient, CHU-SE supplied DICOM images of ten phases throughout the cardiac cycle (resolution: 512x512, slice thickness = 0.5 mm). The lumen of the aneurysm was clearly visible in the DICOM files, but detection of the aneurysm surface was not possible automatically. A non-automatic segmentation of the CT image slices was performed using MIMICS (v. 10.01, Materialise NV). The three-dimensional surface of the aorta in each phase was identified and then the aneurysm was set apart from the remaining aorta. Since the thickness of the aneurysm could not be measured from the images, it was assumed to be constant and equal in its pressure-free configuration to the value measured *ex vivo* for each patient (Table 1). To identify the diastolic and systolic scans, the luminal volume for each phase was calculated. The systolic scan was defined as the one with the largest volume and the diastolic scan as the one with the smallest volume (Figure 2).

The diastolic surface was exported to create the FE model. Rhinoceros (v.4.0, Robert McNeel & Associates), ANSYS ICEM (v.11.0, Ansys Inc) and ABAQUS (Dassault Systèmes Inc.) were used to reconstruct the FE mesh, composed of approximately 40000 hybrid hexahedral structured elements (C3D8H) and 120000 nodes.

To establish the appropriate element size, a mesh independence study was conducted prior to the complete study in order to guarantee that the results were grid

independent. It was clearly demonstrated that for a number of elements greater than 40000, increasing refinements produced higher computational costs but differences in stress of less than 1%.

The dynamic CT scans were also used to measure the patient specific aneurysm volume throughout the cardiac cycle (see Table 2).

To run FE analyses, the first step was to derive the zero-pressure geometry from the diastolic geometry reconstructed from the CT scan. A diastolic pressure of 80 mmHg (10.67 kPa) was assumed for all patients. The zero-pressure geometry was calculated using the pull-back algorithm developed by Riveros et al. [43].

ABAQUS was used to run the FE analyses in the ATAA models. The wall shear stress (WSS) induced by blood flow was not considered as previous studies have found that WSS have a negligible effect on the overall stress analysis [38,39,57]. For each patient, simulations were performed to calibrate the FE systolic volume; varying each time randomly the material properties in an interval based on the experimental data of our previous studies [9,54]. Similar simulations were performed to calibrate the FE mid-cardiac cycle volume of each patient's aneurysm. The zero-pressure geometry found for each patient was used as the initial reference configuration. The material parameters, found by our experimental study or by our inverse method, were implemented in ABAQUS using the user subroutine UHYPER. At the inlet and outlet of the aneurysm only radial displacement was permitted.

The aneurysm was inflated to a mid-cycle pressure of 13.3 kPa (100 mmHg) and then to a systolic pressure of 16 kPa (120 mmHg). One patient, Patient 5, was hypertensive (Table 1). In this case a mid-cycle pressure of 16 kPa and a systolic blood pressure of 23 kPa (174 mmHg) were used based on his blood pressure readings in the month prior to surgery.

3. *Inverse method to identify the ATAA mechanical properties from dynamic CT scans*

The inverse approach is based on the use of a regression model. A regression model is a simplified numerical model linking independent input variables of greater relevance (here the Demiray's parameters) to the output variables (here the aneurysm volume). In this section, a quadratic regression is used but formulated in a multiple linear matrix regression formulation, where the product of factors and the squares of factors are considered as variables of the linear multiple regression. This approach was initially proposed by Neter et al. in 1996 [36] whose objective was to model the behavior of an output variable **y**, using information provided by some values of the independent input variables $\mathbf{x_1}$, $\mathbf{x_2}$, … , $\mathbf{x_n}$.

The multiple linear regression is written as [53]:

$\mathbf{y_i} = \beta_0 + \sum_{j=1}^{k} \beta_j \mathbf{x_{ij}} + \varepsilon_i$, equivalent to the matrix form: **Y** = **X** β + ε,

where $\mathbf{Y} = \begin{pmatrix} y_1 \\ y_2 \\ \vdots \\ y_n \end{pmatrix}$ is an n x 1 vector of variable observations, **X** an n x p design matrix,

$\mathbf{X} = \begin{pmatrix} 1 & x_{11} & \cdots & x_{1(p-1)} \\ \vdots & \vdots & \ddots & \vdots \\ 1 & x_{n1} & \cdots & x_{n(p-1)} \end{pmatrix}$, $\beta = \begin{pmatrix} \beta_1 \\ \beta_2 \\ \vdots \\ \beta_{p-1} \end{pmatrix}$ a p x 1 vector of regression parameters, and

$\varepsilon = \begin{pmatrix} \varepsilon_1 \\ \varepsilon_2 \\ \vdots \\ \varepsilon_n \end{pmatrix}$ the n x 1 vector of additive errors.

The least-squares method is used to adjust a regression line to the data $\{(x_i, y_i)\}_{i=1}^{n}$, where $x_i = \{x_{i,1}, \dots, x_{i,p-1}\}$. Thus, the objective is to find the regression coefficients $\hat{\beta}$ that minimize the following criterion:

$$Q(\beta) = (\mathbf{Y} - \mathbf{X}\beta)^T(\mathbf{Y} - \mathbf{X}\beta) = \sum_{i=1}^{n}(\mathrm{y_i} - \mathrm{x_i}\beta)^2 \qquad (3)$$

Taking derivatives with respect to β, and zeroing them:

$$\frac{dQ}{d\beta} = -2\mathbf{X}^T(\mathbf{Y} - \mathbf{X}\beta) = 0 \Rightarrow (\mathbf{X}^T\mathbf{X})\beta = \mathbf{X}^T\mathbf{Y}; \text{ so } \hat{\beta} = (\mathbf{X}^T\mathbf{X})^{-1}\mathbf{X}^T\mathbf{Y} \qquad (4)$$

Using the multiple linear regression method described previously, the objective is to predict the volume of the aneurysm with respect to the Demiray's parameters (D_1 and D_2 considered as independent factors). The general quadratic equation is applied as a regression model, based on the results of previous simulations which focused on determining the aneurysm's volume.

Assuming that the volume change from diastole to systole and from diastole to cardiac mid-cycle depends only on the Demiray's parameters, the volumetric function may be written as:

$$f(D_1, D_2) = \beta_1 D_1 + \beta_2 D_2 + \beta_3 D_1^2 + \beta_4 D_2^2 + \beta_5 D_1 D_2 + \beta_6 \qquad (5)$$

For each patient, eight FE simulations were performed to find the systolic/mid-cycle volume; varying each time randomly the material properties in their interval of definition. A matrix model linking the information generated by the different computational simulations was generated. With the Minitab® program, a multiple regression using the least squares method was achieved [48].

To determine the model that best predicts the collected information, two indicators were considered: the standard deviation (S), and the quadratic correlation (R-Sq). The best regression corresponds to the lowest (S), while (R-Sq) should tend to 100%. These indicators are provided by Minitab® for each of the generated models.

Eventually, two regression functions describing the aneurysm volume respectively at systole and cardiac mid-cycle are obtained, namely f_{sys} and f_{mid}.

Two cost functions are then defined as F = f – Volume (CT). They should tend to zero so that the volumes given by the regression functions of each patient tend to the CT volumes at systole and cardiac mid-cycle.

Three cases are then distinguished:

a)- Both systolic F_{sys} and mid-cycle F_{mid} cost functions cross each other in two points. Two sets of values for each Demiray parameter are then obtained. Only values included in the experimental interval of variation of both parameters are kept. If both sets of values are valid then only the set leading to positive volumes is kept.

b)- Both systolic and mid-cycle cost functions cross each other in one point. Then only one value is found for D_1 and D_2, and these values are considered as the appropriate mechanical properties for the patient's ATAA.

c)- Both systolic and mid-cycle cost functions do not cross each other. Then the optimum value of F_{sys} is determined using function "fmincon" in Matlab® (constrained minimization). The values of D_1 and D_2 for which F_{sys} is minimal, are taken as the mechanical parameters of the patient's ATAA.

To verify the results given by the retrospective method, the systolic volume predicted by f_{sys} and its actual CT scan counterpart are compared.

Finally, the obtained Demiray's parameters are compared to the ones found experimentally with the bulge-inflation tests.

III. RESULTS

For each patient both volumetric regression functions f_{sys} and f_{mid} were determined. Then, both cost functions F_{sys} and F_{mid} were plotted using Matlab®, and depending on their intersection, D_1 and D_2 were identified.

For Patient 1, the obtained regression functions for systole and mid-cycle are:

$f^1_{sys}(D_1, D_2) = 101301*D_1-140776*D_2-8326*D_1^2+12065*D_2^2+161.51*D_1*D_2+212483$ (6)

$f^1_{mid}(D_1, D_2) = 36804*D_1-48941*D_2-2969*D_1^2+ 4238*D_2^2 -15.14*D_1*D_2+140106$ (7)

The corresponding cost functions cross each other on two valid points but only one sits in the interval [1.68, 10.64]x[1.94, 9.49] (Figure 3). This point corresponds to D_1=4.59 kPa and D_2=4.32.

For Patient 2, the obtained regression functions for systole and mid-cycle are:

$f^2_{sys}(D_1,D_2) =158279*D_1-210503*D_2-12839*D_1^2+18268*D_2^2 +14.49*D_1*D_2+273962$ (8)

$f^2_{mid}(D_1,D_2) =102847*D_1-136701*D_2-8346*D_1^2+11870*D_2^2 +11.37*D_1*D_2+227825$ (9)

The cost functions do not cross each other in the intervals of D_1 and D_2 (Figure 4). Then the values of D_1 and D_2 corresponding to the optimal value of F^2_{sys} are derived, which are 2.98 kPa and 3.16, respectively.

For Patient 3, the obtained regression functions for systole and mid-cycle are:

$f^3_{sys}(D_1, D_2) = 16285*D_1 -21626*D_2 -1310.3*D_1^2+ 1871.7*D_2^2 -9.27*D_1*D_2+ 48922$ (10)

$f^3_{mid}(D_1, D_2) = 10827*D_1 -14382*D_2 -873.8*D_1^2+ 1245.7*D_2^2 -3.34*D_1*D_2+ 43733$ (11)

These two functions cross each other at four points (Figure 5) but only one sits in the intervals. D_1 and D_2 are found equal to 4.64 kPa and 6.71, respectively.

For Patient 4, the obtained regression functions for systole and mid-cycle are:

$f^4_{sys}(D_1,D_2)= 65718*D_1 -87577*D_2 -5329*D_1^2+ 7593*D_2^2 +5.9*D_1*D_2+ 125188$ (12)

$f^4_{mid}(D_1,D_2)= 34962*D_1 -46593*D_2 -2834.8*D_1^2+ 4039.2*D_2^2 +3.02*D_1*D_2+ 99832$ (13)

Optimizing $F^4_{sys} = f^4_{sys} - 81134.05$, D_1 and D_2 are found equal to 3.79 kPa and 3.60, respectively (Figure 6).

For Patient 5, the obtained regression functions for systole and mid-cycle are:

$$f^5_{sys}(D_1, D_2) = 56773*D_1 - 75543*D_2 - 4570*D_1^2 + 6540*D_2^2 - 34.81*D_1*D_2 + 101746 \quad (14)$$

$$f^5_{mid}(D_1, D_2) = 61860*D_1 - 79589*D_2 - 4990*D_1^2 + 6926*D_2^2 - 18.89*D_1*D_2 + 95039 \quad (15)$$

The cost functions cross each other in two points. Only one point presents parameters that lead to positive values of systolic volume. These parameters are D_1= 9.18 kPa and D_2= 3.20 (Figure 7).

A summary of the β_i coefficients defining volumetric function $f(D_1, D_2) = \beta_1 D_1 + \beta_2 D_2 + \beta_3 D_{12} + \beta_4 D_{22} + \beta_5 D_1 D_2 + \beta_6$, for the systolic and mid-cycle phases, is reported in Table 3, whereas the Demiray's parameters found for each patient are reported in Table 4.

A comparison of the stress-stretch response curves in equibiaxial tension predicted with both sets of parameters is shown in Figure 8: one curve is predicted with the material parameters obtained from the experimental tests carried out on the excised samples, and the other curve is predicted with the material parameters identified from the gated CT. In Figure 8, we have also plotted a rough approximation of the states of stresses corresponding to the diastole, the systole and the mid-cycle. These states of stress were estimated using the Law of Laplace and assuming, in a first approximation, each aneurysm as spherical.

Table 3. Recapitulative table of the volumetric function coefficients $f(D_1, D_2) = \beta_1 D_1 + \beta_2 D_2 + \beta_3 D_{12} + \beta_4 D_{22} + \beta_5 D_1 D_2 + \beta_6$, for the systolic and mid-cycle phases.

	Patient ID	β_1	β_2	β_3	β_4	β_5	β_6
Systole	1	101301	-140776	-8326	12065	161.51	212483
	2	158279	-210503	-12839	18268	14.49	273962
	3	16285	-21626	-1310.3	1871.7	-9.27	48922
	4	65718	-87577	-5329	7593	5.9	125188
	5	56773	-75543	-4570	6540	-34.81	101746
Mid-cardiac cycle	1	36804	-48941	-2969	4238	-15.14	140106
	2	102847	-136701	-8346	11870	11.37	227825
	3	10827	-14382	-873.8	1245.7	-3.34	43733
	4	34962	-46593	-2834.8	4039.2	3.02	99832
	5	61860	-79589	-4990	6926	-18.89	95039

Table 4. Summary of the Demiray's parameters found for each patient with the inverse method, predicted volume variations and FE peak wall stresses predictions.

Patient ID	D_1 (kPa)	D_2	Predicted systolic ΔV (%)	FE peak wall stress with predicted parameters (kPa)	FE peak wall stress with experimental parameters (kPa)
1	4.59	4.32	12.93	830	943
2	2.98	3.16	1.79	697	616
3	4.64	6.71	2.45	523	492
4	3.79	3.60	14.62	701	693
5	9.18	3.20	18.73	887	744

For each patient, the Demiray parameters are input in the FE model and a stress analysis is achieved for the systolic pressure (for P1 to P4, systolic pressure is equal to 120 mmHg, whereas for P5, it is 174 mmHg). For the sake of comparison we performed stress analyses using the Demiray parameters that were derived from the bulge-inflation tests and those that were identified using the inverse analysis.

Once the stress analyses were complete for all the patients and for the two sets of Demiray's parameters, the retrospective rupture risk for each patient was determined. The rupture risk index was calculated by dividing the predicted peak wall stress at systole by the experimentally characterized rupture stress (Table 2).

A second criterion was also derived using the FE model, named the overpressure index. This criterion was estimated by dividing the patient's actual systolic pressure

by the burst pressure, which is the luminal pressure required to reach a maximum stress failure criterion in the wall (Figure 9). For both criteria, a value close to 1 indicates a high rupture risk. The maximum diameter criterion was normalized by the cut-off value of 55 mm to provide a diameter criterion that ranges between approximately 0 and 1. The three criteria are presented in Figure 10, for both sets of Demiray parameters (respectively bulge-inflation test and inverse analysis).

The overpressure index and the rupture risk index, found with both sets of Demiray parameters, show very similar tendency. Both of them showed that patient 5 (hypertensive patient) had the highest risk of rupture; which is not in agreement with the aneurysm diameter criterion (Patient 2 had the highest aneurysm diameter).

The percentages of volume changes between the predictions and the CT scans are shown in Figure 11. The maximum relative error between them is 0.6%, which includes the error introduced by the pull-back algorithm (zero-pressure) between the CT scan and the estimated diastolic volume, and the error introduced by the regression method between the CT scan and the predicted systolic volume.

IV. DISCUSSION

The major originality of this study is the patient-specific non-invasive identification of material parameters using in vivo gated CT. It is the first time that an inverse analysis is proposed from gated CT images to identify the patient specific material properties of ATAAs. Similar approaches has been developed and applied successfully on AAAs using ultrasounds [61] or gated CT [41,52]. The latter identified only a linear elastic parameter (compliance) and not hyperelastic parameters, but they were able to do this identification regionally. Relevant identifications are confirmed in our study by the maximal relative error reported between the predicted and the CT systolic

volume, which was 0.019%. Other studies have used cost functions based on geometric similarity to identify material properties in soft tissues, as for instance Largo [27] and Martinez-Martinez [30]. However, the error attributed to their method (19.32% and 6.5%) was much higher than the one attributed to our method (0.6%). This may be explained by the relatively large volume changes, in our case, compared to the voxel size of the CT scans.

Another important originality of our study is that we were able to characterize material parameters of 5 human ATAAs in two ways: first with the inverse method based on the gated CT scans, and second by testing the excised aneurysm in a bulge inflation test. The values found by both methods were similar (Table 4). The stress-stretch response curves in equibiaxial tension obtained with the two sets of material parameters, were also compared (Fig 8). Though they remain close, we can notice some discrepancies between the gated CT curves and the experimental inflation curves. It is interesting to look at these discrepancies especially in the region between diastole and systole, which is a very limited region of the response where the identification from the gated CT is achieved. The average slope in this region is related to the arterial wall stiffness between diastole and systole, which controls the volume changes between diastole and systole estimated from the gated CT. The discrepancies with the experimental curves may result from the conditions of the in vitro tests themselves: only a portion of the tissue was characterized in vitro using a bulge inflation test which may induce a slightly different response with the in vivo response.

However, the same tendencies were found. For instance Patient 2 and Patient 3 here have both a lower compliance. It corroborates that Patient 3 has the highest values of D_2. For Patient 2, the material properties are lower but there is a very large

deformation between the physiological configuration and the zero-pressure configuration for this aneurysm.

After identifying material parameters, a FE stress analysis was performed for each of the 5 ATAAs and the aneurysm rupture risk was estimated for the five patients on the day of their surgical intervention. A few assumptions were made to reconstruct the FE models: only the ascending part of the aorta (between the aortic root and the aortic arch) was modelled, a uniform thickness and uniform material properties were assumed in each case, the blood action was limited to a uniform luminal pressure neglecting the perivascular pressure, and the length of the modelled aortic segment was maintained constant during pressure changes. The derivation of aneurysm rupture risk showed that the material parameters obtained from gated CT or from experimental bulge inflation provided very similar results (Fig. 4).

However, in order to derive a truly patient specific rupture risk from patient-specific FE stress analyses, patient-specific wall thicknesses and patient-specific wall strengths would also be required. Here they were obtained retrospectively as the tissues were characterized in vitro after ATAA repair.

Regarding the thickness, the current resolution of CT scans is not sufficient to measure it, contrarily to AAA where the thickened wall can be resolved [49].

Regarding the strength, it would be important to characterize it non-invasively *in vivo* preoperatively and regionally as it may vary between patients [16] and positions [47]. Recent studies have tried to correlate the strength to other biomarkers. It is known that localized ‘hot spots’ of matrix metalloproteinase (MMP) hyperactivity may lead to local weakening of the aneurysm wall [55], impairing mechanosensing [22]. Reeps et al. [41] used a contrast enhanced 18F-fluorodeoxyglucose-positron emission

tomography/CT (FDG-PET/CT) to determine the Matrix Metalloproteinase activity and strength. This technique bears great potential for non-invasive estimation of aortic wall properties. It has the potential to identify local pathological activities and act as a surrogate marker of material strength [41, 51, 58]. Thus, local metabolic activity measured by FDG-PET/CT can provide valuable information on the distribution of mechanical properties. However, an increase in the metabolic activity does not lead systematically to higher rupture stress [41]. Ongoing inflammation may also account for aneurysm weakening and could characterize the tissue strength [42].

Another assumption raised by several authors [2,11,26] is that the stiffness of tissues from ATAAs may be positively correlated with the strength. Therefore if this assumption was confirmed, using gated CT and our inverse approach to identify material parameters, we would be able to estimate the strength.

Another important requirement of patient specific FE analyses for ATAAS is the boundary conditions. An improvement for patient-specific FE analyses would be using 4D MRI which permits quantifying the flow field, enabling the identification of pressure gradients in the aorta [29]. This information could be used to improve the boundary conditions applied in the model. Moreover, 4D MRI would permit tracking the axial motions of the wall and apply more realistic assumptions for the axial boundary conditions. To translate the approach to the clinical setting, the 4D MRI would also be a nice alternative to the ECG gated dynamic CT scan as the ECG gated dynamic CT scan is only achieved preoperatively for the purpose of planning the surgical operation, but it could not be repeated several times due to X-ray radiations.

A question that can be asked is whether patient specific material properties are required for performing patient-specific FE stress analyses in an aortic aneurysm [46]. In general, patient-specific material properties are required for structural analyses. But in the particular case of aneurysms where the geometry is provided in the loaded state, then Miller and Lu [34, 62] have shown that the stress analysis can be derived without knowing the material properties, and provided that the aneurysm can be modelled as a membrane. This is in agreement with our results showing that both sets of material parameters (CT gated and bulge inflation) provided very similar peak wall stresses despite their relative differences.

However, identifying patient specific material properties for ATAAs still deserves important interest. First, it becomes more and more common to perform growth and remodeling computational analyses for aortic aneurisms [31, 49, 60]. The impact of material properties for these computational analyses may be considerable [60]. Also an assumption raised by several authors [2,11,26] is that the stiffness of tissues from ATAAs may be positively correlated with the strength. So obtaining non-invasively the patient-specific material properties may represent a very important interest.

Despite encouraging results, this study presents a number of limitations which are currently being addressed in another clinical protocol recently started at CHU-SE: (1) only five patients were included, (2) the CT scans were manually segmented which is a time consuming operation, (3) pressure measurements taken before surgery were not available for two of the five selected patients, and for some of them, there were several measurements with considerable variations (Table 1). (4) uniform, monolayer and isotropic constitutive behavior of the aortic wall was assumed, (5) the FE model only included the aneurysm and not its proximal (aortic root) nor its distal part (aortic arch and descending thoracic aorta), (6) the boundary conditions of the FE model did

not include motions of the proximal and distal parts of the aneurysm during a cardiac cycle, (7) the axial elastic recoil during aneurysm collection was not measured by the surgeons.

REFERENCES

[1] Avril, S., Evans, S., Miller, K. Inverse problems and material identification in tissue biomechanics. Journal of the mechanical behavior of biomedical materials. Elsevier, 27: 129 – 131. 2013.

[2] Azadani, A. N., S. Chitsaz, A. Mannion, A. Mookhoek, A. Wisneski, J. M. Guccione, M. D. Hope, L. Ge, and E. E. Tseng. Biomechanical properties of human ascending thoracic aortic aneurysms. Ann. Thorac. Surg. 96:50–58. 2013.

[3] Badel, P.; Avril, S.; Lessner, S.; Sutton, M.; Mechanical identification of layer-specific properties of mouse carotid arteries using 3D-DIC and a hyperelastic anisotropic constitutive model, Computer methods in biomechanics and biomedical engineering.15 (1): 37-48. 2012.

[4] Carew, T.E., Vaishnav, R.N., Patel, D.J. Compressibility of the Arterial Wall. Circ. Res. 23: 61–68, 1968.

[5] Chau, K. H., and Elefteriades, J. A. Natural history of thoracic aortic aneurysms: size matters, plus moving beyond size. Prog. Cardiovasc. Dis. 56(1): 74–80, 2013.

[6] Coady, M. A., Rizzo, J. A., Hammond, G. L., Kopf, G. S., and Elefteriades, J. A. Surgical Intervention Criteria for Thoracic Aortic Aneurysms : A Study of Growth Rates and Complications. Ann. Thorac. Surg. 67: 1922–1926, 1999.

[7] Coady, M. A., Rizzo, J. a, Hammond, G. L., Mandapati, D., Darr, U., Kopf, G. S., and Elefteriades, J. A. What is the appropriate size criterion for resection of thoracic aortic aneurysms?. J. Thorac. Cardiovasc. Surg. 113(3): 476–91, 1997.

[8] Davies, R. R., Goldstein, L. J., Coady, M. A., Tittle, S. L., Rizzo, J. A., Kopf, G. S., and Elefteriades, J. A. Yearly Rupture or Dissection Rates for Thoracic Aortic Aneurysms : Simple Prediction Based on Size. Ann. Thorac. Surg. 73: 17–28, 2002.

[9] Davis, F.M., Luo, Y., Avril, S., Duprey, A., Lu, J. Pointwise characterization of the elastic properties of planar soft tissues: application to ascending thoracic aneurysms. Biomechanics and modeling in mechanobiology. In press, 2015.

[10] Demiray, H. A note on the elasticity of soft biological tissues. J. Biomech. 5: 309–311,1972.

[11] Di Martino ES, Bohra A, Vande Geest JP, Gupta N, Makaroun MS, Vorp DA. Biomechanical properties of ruptured versus electively repaired abdominal aortic aneurysm wall tissue. J Vasc Surg. 43 :570–576. 2006.

[12] Doyle, B. J., Cloonan, A. J., Walsh, M. T., Vorp, D. A., McGloughlin, T. M. Identification of rupture locations in patient-specific abdominal aortic

aneurysms using experimental and computational techniques. J. Biomechanics. 43 (7): 1408–1416. 2010.

[13] Doyle , B. J., Killion, J., Callanan, A. Use of the photoelastic method and finite element analysis in the assessment of wall strain in abdominal aortic aneurysm models. J. Biomechanics. 45 (10): 1759–1768. 2012.

[14] Elefteriades, J., and Farkas, E. Thoracic aortic aneurysm clinically pertinent controversies and uncertainties. J. Am. Coll. Cardiol. 55(9): 841–57, 2010.

[15] Fillinger, M. F., Marra, S. P., Raghavan, M. L., and Kennedy, F. E. Prediction of rupture risk in abdominal aortic aneurysm during observation: wall stress versus diameter. J. Vasc. Surg., 37(4): 724–32, 2003.

[16] Forsell, C., Björck, H.M., Eriksson, P., Fraco-Cereceda, A., Gasser, T.C. Aneurysmal Wall: Differences Between Bicuspid Aortic Valve and Tricuspid Aortic Valve Patients. Annals of Thoracic Surgery. In press, 2014.

[17] Franquet, A., Avril, S., Le Riche, R., Badel, P., Schneider, F.C., Yong Li, Z., Boissier, C., Favre, J.P. A New Method for the In Vivo Identification of Mechanical Properties in Arteries From Cine MRI Images: Theoretical Framework and Validation. IEEE Transactions on medical imaging, 32(8), 2013.

[18] Franquet, A., Avril, S., Le Riche, R., Badel, P. Identification of heterogeneous elastic properties in stenosed arteries: a numerical plane strain study. Computer Methods in Biomechanics and Biomedical Engineering. 15(1), 2012.

[19] Frydrychowicz, A., Stalder, A. F., Russe, M. F., Bock, J., Bauer, S., Harloff, A., Berger, A., Langer, M., Hennig, J., Markl, M. Three-dimensional analysis of segmental wall shear stress in the aorta by flow-sensitive four-dimensional-MRI. J. of Magnetic Resonance Imaging. 30(1): 77–84, 2009.

[20] Hartnell, G. G. Imaging of Aortic Aneurysms and Dissection: CT and MRI. Journal of Thoracic Imaging. 16: 35–46, 2001.

[21] Humphrey, J. Cardiovascular Solid Mechanics: Cells, Tissues, and Organs. Springer, New York. 2002.

[22] Humphrey, J.D., Milewicz, D.M., Tellides, G., Schwartz, M.A. Dysfunctional Mechanosensing in Aneurysms. Science. 344(477), 2014.

[23] Johansson, G., Markström, U., and Swedenborg, J. Ruptured thoracic aortic aneurysms: a study of incidence and mortality rates. J. Vasc. Surg. 21(6): 985–8, 1995.

[24] Juvonen, T., Ergin, M. A., Galla, J. D., Lansman, S. L., Nguyen, K. H., Mccullough, J. N., Levy, D., de Asla, R. A., Bodian, C. A., and Griepp, R. B. Prospective Study of the Natural History of Thoracic Aortic Aneurysms. Ann. Thorac. Surg. 4975(97):1533–45, 1997.

[25] Kim, J. H., Avril, S., Duprey, A., Favre, J. P. Experimental characterization of rupture in human aortic aneurysms using a full-field measurement technique. Biomechanics and Modeling in Mechanobiology. 11(6): 841-853. 2012.

[26] Kontopodis, N.; Georgakarakos, E.; Metaxa, E.; Pagonidis, A.; Papaharilaou, Y.; Yoannou, C.V.; Estimation of wall properties and wall strength of aortic

aneurysms using modern imaging techniques. One more step towards a patient-specific assessment of aneurysm rupture risk, Medical Hypotheses,81,212-215,2013.

[27] Lago, M. A., Ruperez, M. J., Martinez-Martinez, F., and Monserrat, C. Genetic algorithms for estimating the biomechanical behavior of breast tissues. Biomedical and Health Informatics (BHI), 2014 IEEE-EMBS International Conference on: 760 – 763, 2014.

[28] Lu , J., Zhou, X., Raghavan, M. L. Inverse elastostatic stress analysis in pre-deformed biological structures: Demonstration using abdominal aortic aneurysms. Journal of Biomechanics. 40(3): 693–696, 2007.

[29] Markl, M., Kilner, P. J., Ebbers, T. Comprehensive 4D velocity mapping of the heart and great vessels by cardiovascular magnetic resonance. J. of Cardiovascular Magnetic Resonance, 13(7): 1-22, 2011.

[30] Martínez-Martínez, F., Rupérez, M. J., Martín-Guerrero, J. D., Monserrat, C., Lago, M. A., Pareja, E., Brugger, S., and López-Andújar, R. Estimation of the elastic parameters of human liver biomechanical models by means of medical images and evolutionary computation. Comput. Methods Programs Biomed. 111(3): 537–49, 2013.

[31] Martufi, G., Auer, M., Roy, J., Swedenborg, J., Sakalihasan, N., Panuccio, G., Gasser, T.C. Multidimensional growth measurements of abdominal aortic aneurysms. J Vasc Surg. 58(3):748-55, 2013.

[32] Martufi, G., Gasser, T.C., Appoo, J.J., Di Martino, E.S. Mechano-biology in the thoracic aortic aneurysm: a review and case study. Biomechanics and modeling in mechanobiology. 13(5):917-928, 2014.

[33] McGloughlin, T. Biomechanics and Mechanobiology of Aneurysms. Springer-Verlag Berlin Heidelberg. ISSN 1868-2006 / ISBN 978-3-642-18094-1. 2011.

[34] Miller, K., Lu, J. On the prospect of patient-specific biomechanics without patient-specific properties of tissues. Journal of the Mechanical Behavior of Biomedical Materials. 27:154-166, 2013.

[35] Nelder, J. A., Mead, R. A Simplex Method for Function Minimization. The Computer Journal. 7(4):308-313, 1965.

[36] Neter, J., Kutner, M., Wasserman, W., Nachtsheim, C. Applied linear statictical models. Edition Mc Graw Hill, 1996.

[37] O'Leary, S. A, Doyle, B. J, McGloughlin, T. M. Comparison of methods used to measure the thickness of soft tissues and their influence on the evaluation of tensile stress. J Biomech. 46(11):1955-60. 2013.

[38] Peattie, R.A., Asbury, C.L., Bluth, E.I., Riehle, T.J. Steady flow in models of abdominal aortic aneurysms. Part II: Wall stresses and their implication for in vivo thrombosis and rupture. J. Ultrasound Med. 15: 689–696, 1996.

[39] Peattie, R.A., Riehle, T.J., Bluth, E.I. Pulsatile Flow in Fusiform Models of Abdominal Aortic Aneurysms: Flow Fields, Velocity Patterns and Flow-Induced Wall Stresses. J. Biomech. Eng. 126(4): 438-446, 2004.

[40] Raghavan, M.L., Vorp, D. A., Federle, M. P., Makaroun, M. S., Webster, M. W. Wall stress distribution on three-dimensionally reconstructed models of human abdominal aortic aneurysm. Journal of Vascular Surgery. 31(4): 760–769, 2000.

[41] Reeps, C., Maier, A., Pelisek, J., Härtl, F., Grabher-Meier, V., Wall, W. A., Essler, M., Eckstein, H.-H., Gee, M. W. Measuring and modeling patient-specific distributions of material properties in abdominal aortic aneurysm wall. Biomech Model Mechanobiol. 12(4):717-33, 2013.

[42] Richards, J.M., Semple, S.I., MacGillivray, T.J., Gray, C., Langrish, J.P., Williams, M., Dweck, M., Wallace, W., McKillop, G., Chalmers, R.T., Garden, O.J., Newby, D.E. Abdominal aortic aneurysm growth predicted by uptake of ultrasmall superparamagnetic particles of iron oxide: A pilot study. Circulation Cardiovascular Imaging. 4: 274-281, 2011.

[43] Riveros, F., Chandra, S., Finol, E.A., Gasser, T.C., Rodrigues, J.F. A pull-back algorithm to determine the unloaded vascular geometry in anisotropic hyperelastic AAA passive mechanics. Ann. Biomedial Eng. 41: 694–708, 2013.

[44] Riveros, F., Martufi, G., Gasser, T. C., Rodriguez-Matas, J. F. On the Impact of Intraluminal Thrombus Mechanical Behavior in AAA Passive Mechanics. Annals of Biomedical Engineering. 2015.

[45] Roccabianca, S., Bellini, C., Humphrey, J. D. Computational modelling suggests good, bad and ugly roles of glycosaminoglycans in arterial wall mechanics and mechanobiology. Journal of the Royal Society interface. 11(97):20140397. 2014.

[46] Rodriguez, J.F., Martufi, G., Doblaré, M., Finol, E.A. The effect of material model formulation in the stress analysis of abdomnal aortic aneurysms. Annals of Biomedical Engineering. 37(11), 2009.

[47] Romo, A., Badel, P., Duprey, A., Favre, J.-P., and Avril, S. In vitro analysis of localized aneurysm rupture. J. Biomech. 47(3): 607–616, 2014.

[48] Ryan B. Minitab Software. State College, Pensilvania, 1972.

[49] Shang, E. K., Lai, E., Pouch, A. M., Hinmon, R., Gorman, R. C., Gorman III, J. H., Sehgal, C. M., Ferrari, G., Bavaria, J. E., Jackson, B. M. Validation of semiautomated and locally resolved aortic wall thickness measurements from computed tomography. Journal of Vascular Surgery. 61(4): 1034–1040, 2015.

[50] Sundt, T. M. Indications for aortic aneurysmectomy: too many variables and not enough equations?. J. Thorac. Cardiovasc. Surg. 145(3 Suppl): S126–9, 2013.

[51] Teng, Z.; Feng, J.; Zhang, Y.; Huang, Y.; Sutcliffe, M.P.F.; Brown, A.J.; Jing, Z.; Gillard, J.H.; Lu, Q.; Layer-and Direction-Specific Material Properties, Extreme Extensibility and Ultimate Material Strength of Human Abdominal Aorta and Aneurysm: A Uniaxial Extension Study. Annals of biomedical engineering.1-15. 2015.

[52] Tierney, A. P., Callanan, A., McGloughlin, T. M. Use of Regional Mechanical Properties of Abdominal Aortic Aneurysms to Advance Finite Element Modeling of Rupture Risk. Journal of Endovascular Therapy: 19 (1): 100-114. 2012.

[53] Trabelsi, O., López Villalobos, J. L., Ginel, A., Barrot Cortes, E., Doblaré, M. A pre-operative planning for endoprosthetic human tracheal implantation: a

decision support system based on robust design of experiments. Computer Methods in Biomechanics and Biomedical Engineering, 17(7):750-67, 2012.

[54] Trabelsi, O., Davis, F.M., Rodriguez-Matas, J.F., Duprey, A., Avril, S. Patient specific stress and rupture analysis of ascending thoracic aneurysms. Journal of Biomechanics. In press, 2015.

[55] Vallabhaneni, S.R., Gilling-Smith, G.L., How, T.V., Carter, S.D., Brennan, J.A., Harris, P.L. Heterogeneity of tensile strength and matrix metalloproteinase activity in the wall of abdominal aortic aneurysms. Journal of Endovascular Therapy. 11: 494502, 2004.

[56] Vande Geest, J. P., Di Martino, E. S., Bohra, A., Makaroun, M. S., and Vorp, D. A. A biomechanics-based rupture potential index for abdominal aortic aneurysm risk assessment: demonstrative application. Ann. N. Y. Acad. Sci. 1085: 11–21, 2006.

[57] Vorp, D.A. Biomechanics of abdominal aortic aneurysm. J. Biomech. 40: 1887–1902, 2007.

[58] Vorp, D.A., Schiro, B.J., Ehrlich, M.P., Juvonen, T.S., Ergin, M.A., Griffith, B.P. Effect of aneurysm on the tensile strength and biomechanical behavior of the ascending thoracic aorta. Annals of Thoracic Surgery. 75:1210-1214, 2003.

[59] Wang, D. H. J., Makaroun, M. S., Webster, M. W., Vorp, D. A. Effect of intraluminal thrombus on wall stress in patient-specific models of abdominal aortic aneurysm. Journal of Vascular Surgery. 36 (3): 598–604, 2002.

[60] Wilson, J.S., Baek, S., Humphrey, J.D. Importance of initial aortic properties on the evolving regional anisotropy, stiffness and wall thickness of human abdominal aortic aneurysms. J. R. Soc. Interface. 9(74):2047-58, 2012.

[61] Wittek, A., Karatolios, K., Bihari, P., Schmitz-Rixen, T., Moosdorf, R., Vogt, S., Blase C. In vivo determination of elastic properties of the human aorta based on 4D ultrasound data. J Mech Behav Biomed Mater. 27:167-83. 2013.

[62] Zhao, X., Chen, X., Lu, J. Pointwise Identification of Elastic Properties in Nonlinear Hyperelastic Membranes—Part II: Experimental Validation. J. Appl. Mech. 76: 061014, 2009.

Table legends

Table 1. Patient demographic information.

Table 2. Patient specific material properties and aneurysm volumes during systolic and mid-cardiac cycle phases

Table 3. Coefficients of volumetric function $f(D_1, D_2) = \beta_1 D_1 + \beta_2 D_2 + \beta_3 D_{12} + \beta_4 D_{22} + \beta_5 D_1 D_2 + \beta_6$, for the systolic and mid-cycle phases.

Table 4. Summary of the Demiray's parameters found for each patient with the inverse method, systolic volume, diastolic volume and peak wall stresses predictions.

Table 1. Patient demographic information

Patient ID	Sex/Age	Pre-surgical CT diameter (mm)	Ex-vivo thickness (mm)	Pathologies
1	M/55	55	2.38	AI, bicuspid aortic valve
2	F/76	65	2.44	AI
3	M/79	52	1.76	AI, coronary artery disease, myocardial infarction
4	M/40	55	1.59	AI, bicuspid aortic valve
5	M/72	51	1.90	AI, coronary artery disease, hypertension

Aortic insufficiency (AI)

Table 2. Patient specific material properties identified using the bulge-inflation test and aneurysm CT volumes at diastole, systole and cardiac mid-cycle.

Patient ID	D_1 (kPa)	D_2	ε	Rupture Stress (MPa)	CT systolic volume (mm^3)	CT mid-cycle volume (mm^3)	CT Diastolic volume (mm^3)
1	$8.684^{+0.211}_{-0.205}$	$2.031^{\pm 0.027}$	0.041	1.05 (n=2)	122179.43	113824.41	108145.73
2	$1.766^{+0.081}_{-0.078}$	$6.932^{+0.194}_{-0.19}$	0.034	1.31 (n=4)	148528.18	147401.1	145898.62
3	$4.722^{+0.196}_{-0.191}$	$9.131^{+0.359}_{-0.356}$	0.088	0.95 (n=1)	35131.60	34626.79	34288.73
4	$9.397^{+0.305}_{-0.299}$	$1.972^{\pm 0.031}$	0.063	2.33 (n=2)	81134.05	74712.93	70774.30
5	$10.33^{+0.31}_{-0.29}$	$5.265^{+0.138}_{-0.135}$	0.030	0.76* (n=2)	62086.99	58168.01	52277.81

*The sample ruptured at the border

Table 3. Coefficients of volumetric function f (D_1, D_2) = β_1 D_1+ β_2 D_2 + β_3 D_{12} + β_4 D_{22} + β_5 D_1 D_2 + β_6, for the systolic and mid-cycle phases.

	Patient ID	β_1	β_2	β_3	β_4	β_5	β_6
Systole	1	101301	-140776	-8326	12065	161.51	212483
	2	158279	-210503	-12839	18268	14.49	273962
	3	16285	-21626	-1310.3	1871.7	-9.27	48922
	4	65718	-87577	-5329	7593	5.9	125188
	5	56773	-75543	-4570	6540	-34.81	101746
Mid-cardiac cycle	1	36804	-48941	-2969	4238	-15.14	140106
	2	102847	-136701	-8346	11870	11.37	227825
	3	10827	-14382	-873.8	1245.7	-3.34	43733
	4	34962	-46593	-2834.8	4039.2	3.02	99832
	5	61860	-79589	-4990	6926	-18.89	95039

Table 4. Summary of the Demiray's parameters found for each patient with the inverse method, systolic volume, diastolic volume and peak wall stresses predictions.

Patient ID	D_1 (kPa)	D_2	Predicted systolic volume (mm^3)	Predicted diastolic volume (mm^3)	FE peak wall stress with predicted parameters (kPa)	FE peak wall stress with experimental parameters (kPa)
1	4.59	4.32	122179.53	108194.56	830	943
2	2.98	3.16	148526.27	145913.16	697	616
3	4.64	6.71	35131.46	34291.55	523	492
4	3.79	3.60	81136.05	70790.07	701	693
5	9.18	3.20	62074.87	52283.53	887	744

Figure legends

Figure 1. Experimental setup of the bulge inflation test and test sample (a) immediately after surgical resection and (b) after rupture in the bulge inflation device.

Figure 2. Patient specific aneurysm geometry extraction. (A) DICOM CT image with the aorta in green. (B) Segmented aorta at one phase of the cardiac cycle. (C) Quadratic mesh of the aneurysmal aortic 3D model at the diastolic phase. (D) Quadratic mesh of the aneurysmal aortic 3D model at the systolic phase.

Figure 3: F_{sys} and F_{mid} for Patient 1.

Figure 4: F_{sys} and F_{mid} for Patient 2.

Figure 5: F_{sys} and F_{mid} for Patient 3.

Figure 6: F_{sys} and F_{mid} for Patient 4.

Figure 7: F_{sys} and F_{mid} for Patient 5.

Figure 8: A comparison of the stress-stretch response curves in equibiaxial tension with the two sets of parameters (experimental tests and gated CT).

Figure 9: Luminal pressure required to reach the maximum stress failure criterion: it is determined as the pressure where the FE stress curves cross the horizontal curves (the experimentally measured rupture stress).

Figure 10: Retrospective rupture risk assessments (a) rupture risk index using Demiray's parameters found by regression (Light blue), (b) rupture risk index using experimental Demiray's parameters (Blue) (c) overpressure risk estimate from experimental mechanical properties (Red), (d) overpressure risk estimate from

regression mechanical properties (Light red) and (e) relative diameter (dmax/65). The rupture risk at 5 is calculated using the high systolic pressure of 174 mmHg.

Figure 11: Comparison between actual (blue) and predicted (red) percent volume change of the aneurysm between diastole and systole for each patient.

Figure 1

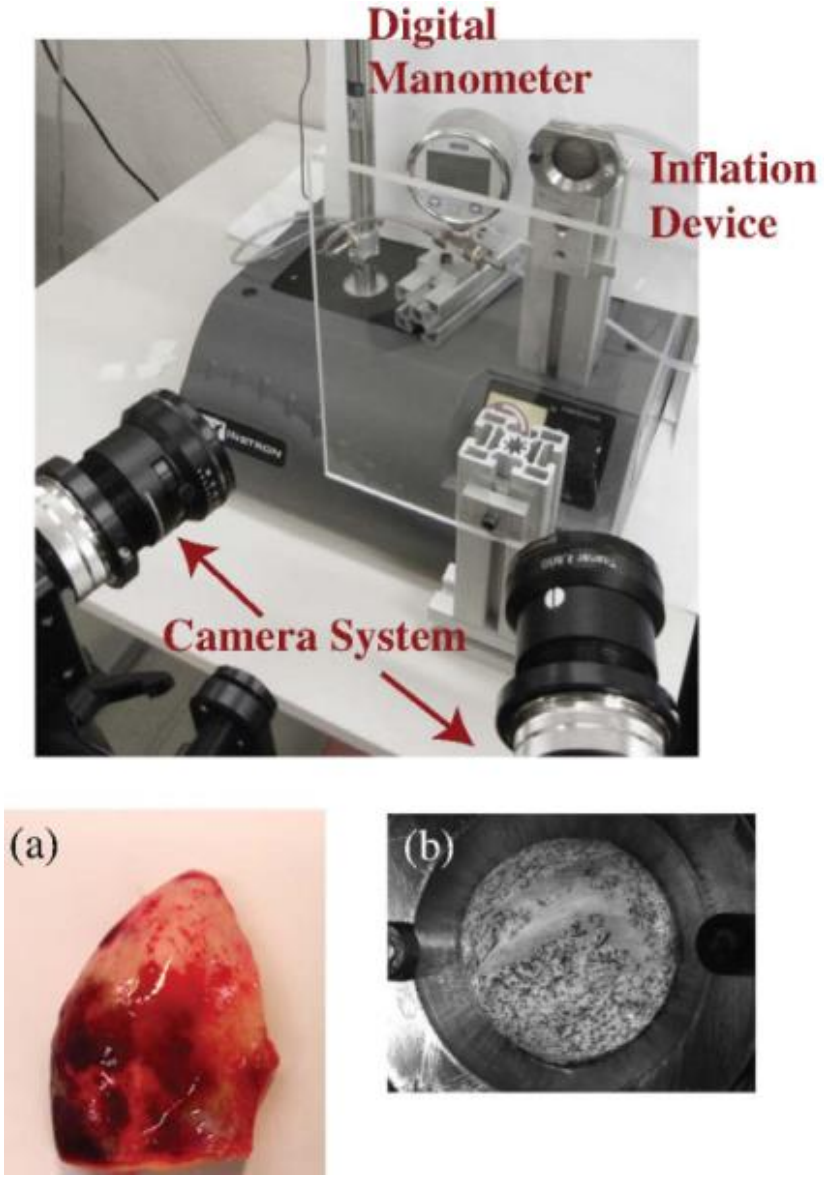

Figure 2

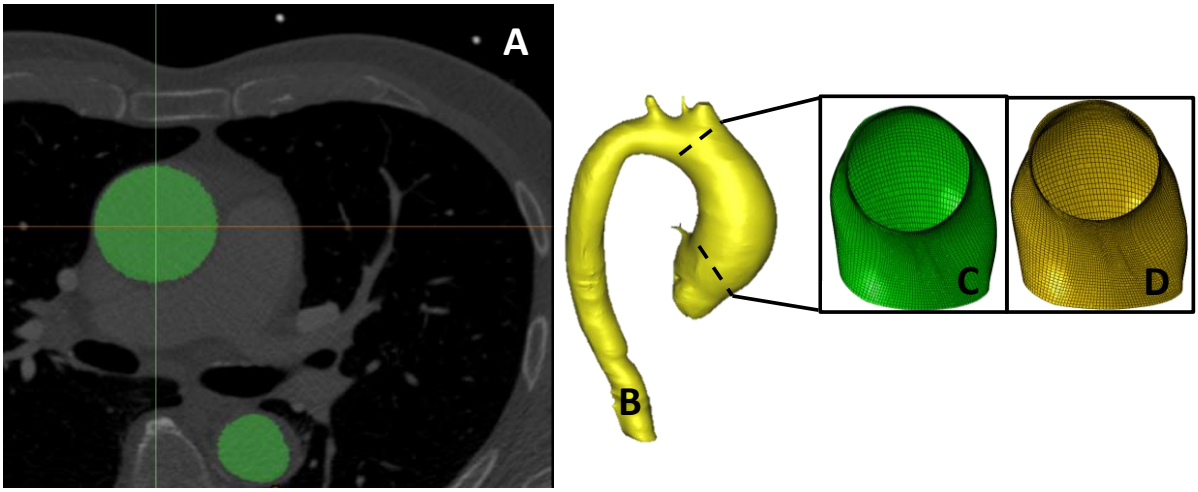

Figure 3

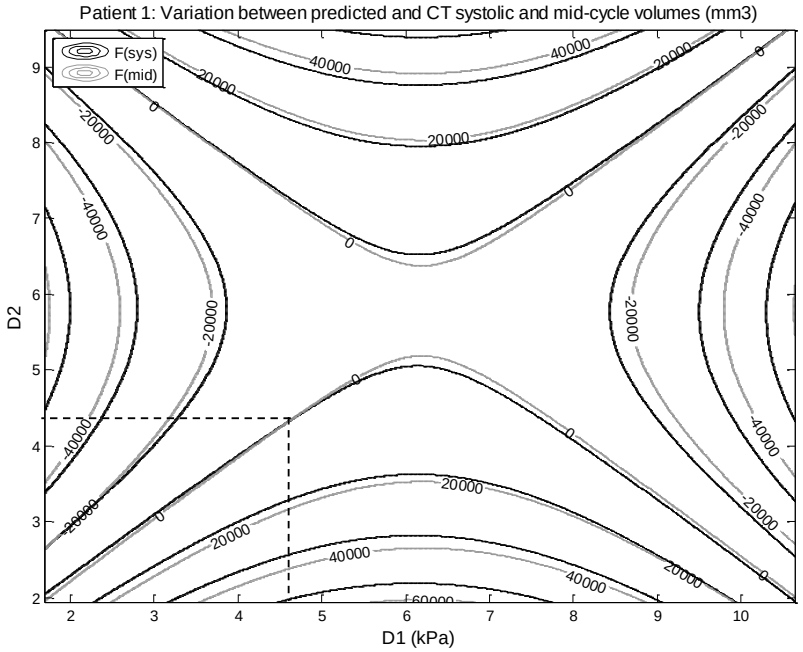
Patient 1: Variation between predicted and CT systolic and mid-cycle volumes (mm3)
F(sys)
F(mid)
D2
D1 (kPa)
40000
20000
0
-20000
-40000
60000

Figure 4

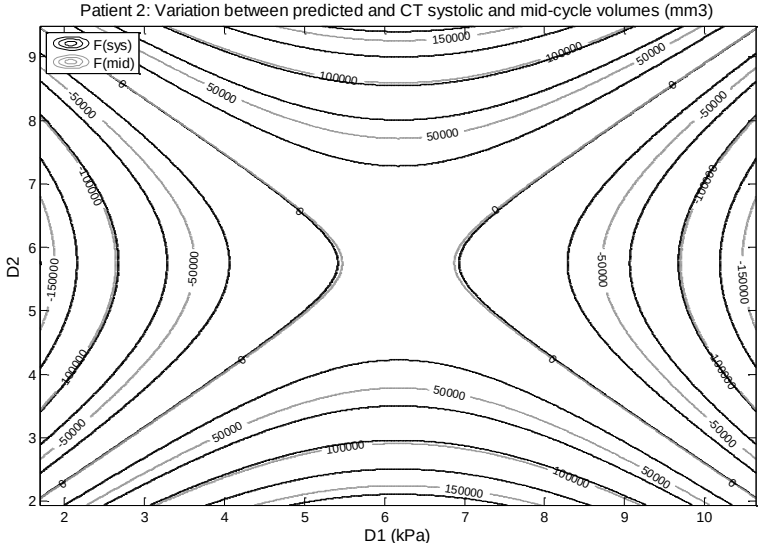
Patient 2: Variation between predicted and CT systolic and mid-cycle volumes (mm3)
F(sys)
F(mid)
D2
D1 (kPa)

Figure 5.

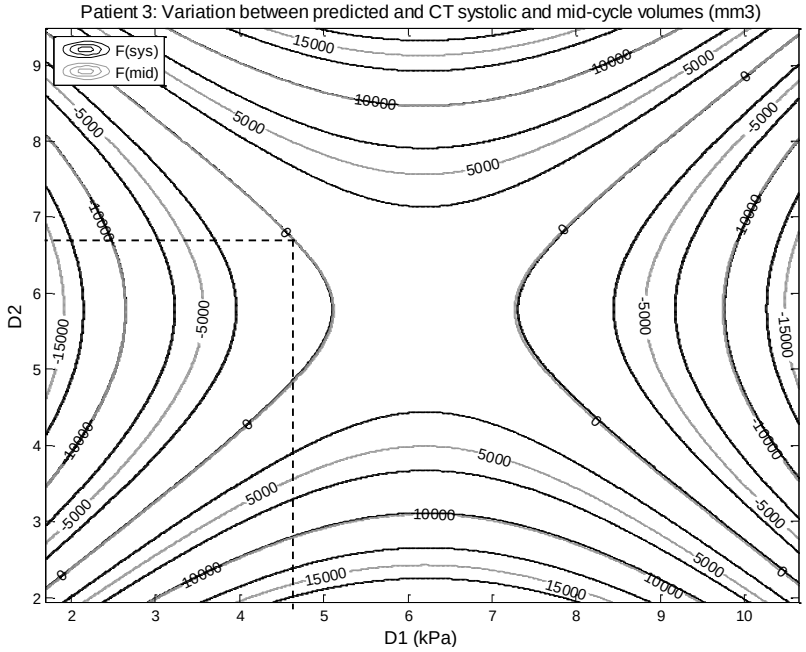
Patient 3: Variation between predicted and CT systolic and mid-cycle volumes (mm3)
F(sys)
F(mid)
D2
D1 (kPa)

Figure 6

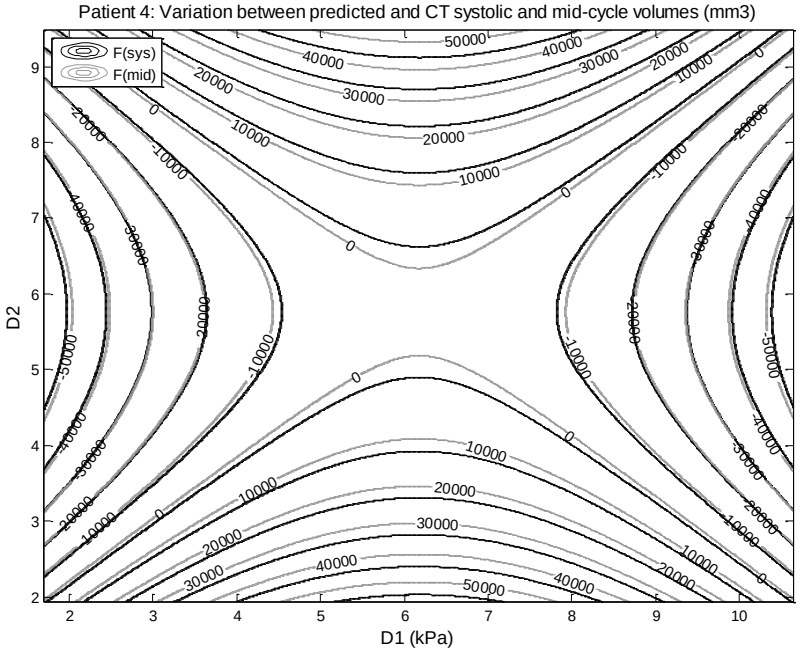
Patient 4: Variation between predicted and CT systolic and mid-cycle volumes (mm3)
F(sys)
F(mid)
D2
D1 (kPa)

Figure 7

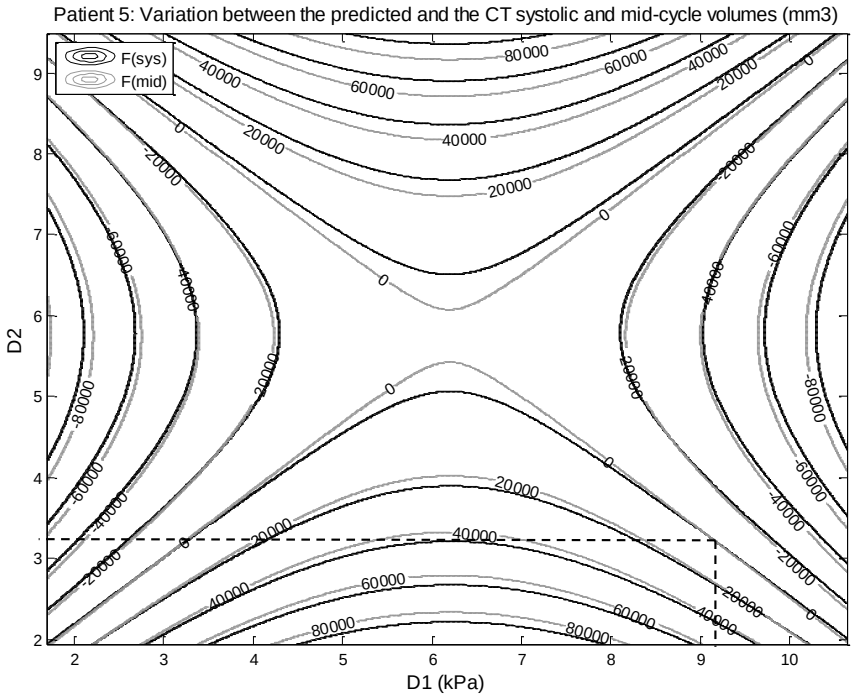
Patient 5: Variation between the predicted and the CT systolic and mid-cycle volumes (mm3)
F(sys)
F(mid)
D2
D1 (kPa)

Figure 8

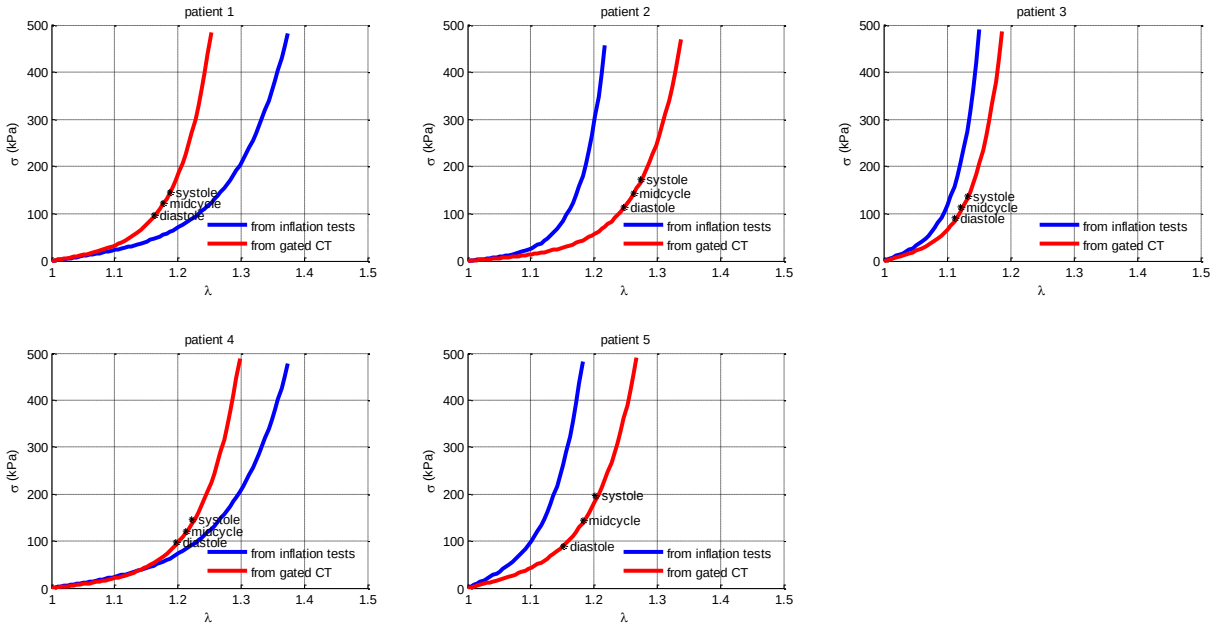
patient 1
patient 2
patient 3
patient 4
patient 5
σ (kPa)
λ
systole
midcycle
diastole
from inflation tests
from gated CT

Figure 9

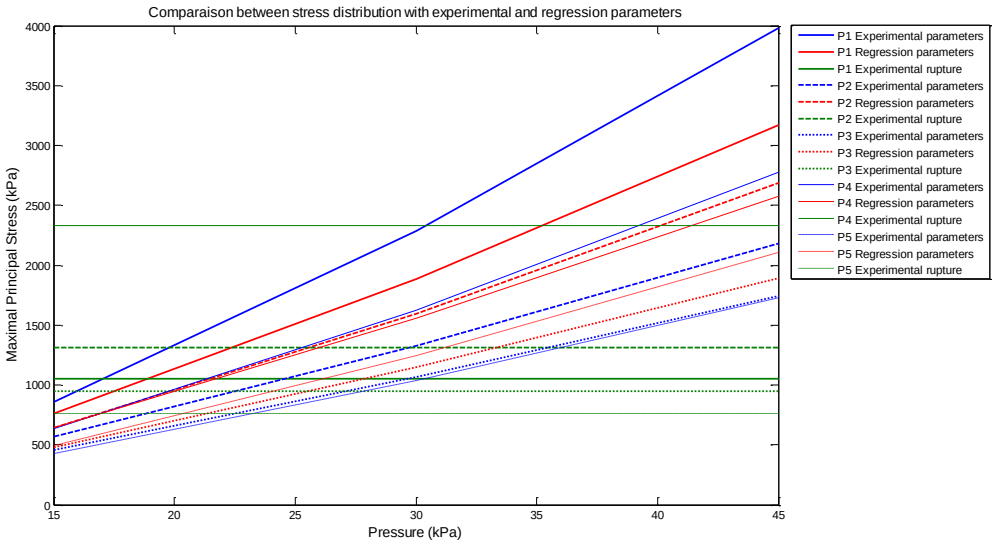
Comparaison between stress distribution with experimental and regression parameters
Maximal Principal Stress (kPa)
Pressure (kPa)
0
500
1000
1500
2000
2500
3000
3500
4000
15
20
25
30
35
40
45
P1 Experimental parameters
P1 Regression parameters
P1 Experimental rupture
P2 Experimental parameters
P2 Regression parameters
P2 Experimental rupture
P3 Experimental parameters
P3 Regression parameters
P3 Experimental rupture
P4 Experimental parameters
P4 Regression parameters
P4 Experimental rupture
P5 Experimental parameters
P5 Regression parameters
P5 Experimental rupture

Figure 10

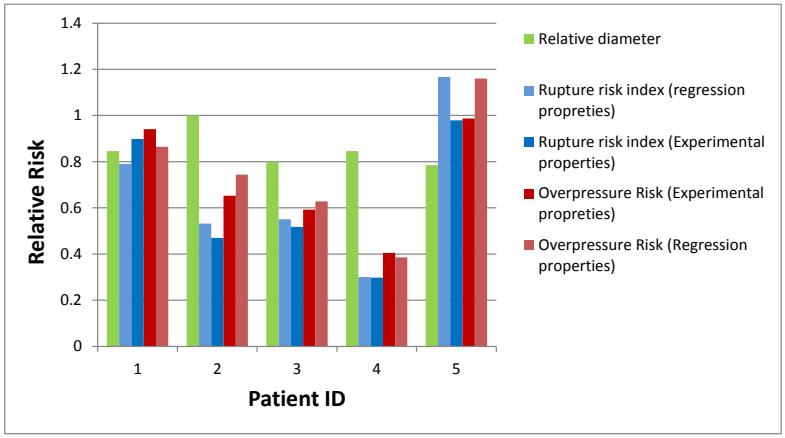
1.4
1.2
1
0.8
0.6
0.4
0.2
0
Relative Risk
1
2
3
4
5
Patient ID
Relative diameter
Rupture risk index (regression propreties)
Rupture risk index (Experimental properties)
Overpressure Risk (Experimental propreties)
Overpressure Risk (Regression properties)

Figure 11

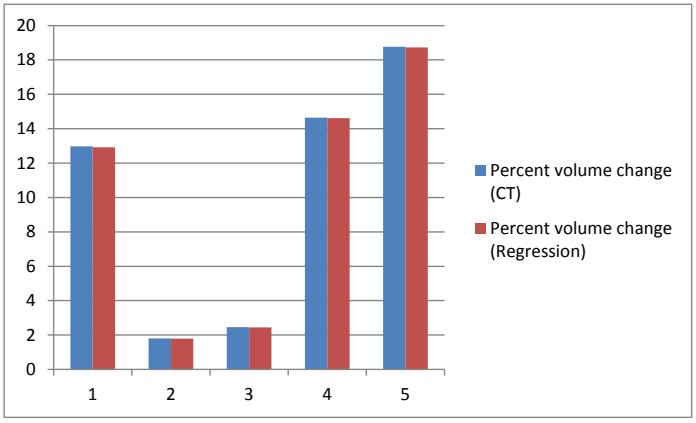
20
18
16
14
12
10
8
6
4
2
0
1
2
3
4
5
Percent volume change (CT)
Percent volume change (Regression)